RSC Advances

ROYAL SOCIETY OF CHEMISTRY

www.rsc.org/advances

Facile synthesis of Ag_2O/N-doped helical carbon nanotubes with enhanced visible-light photocatalytic activity

Jinjuan Xue, ‡ Shuaishuai Ma,‡ Yuming Zhou, * Zewu Zhang, Xin Wu, Chenguang She

School of Chemistry and Chemical Engineering, Southeast University, Nanjing 211189, P. R. China

Abstract: Novel Ag_2O/N-doped helical carbon nanotubes (Ag_2O/N-HCNTs) were successfully synthesized via a simple coprecipitation method and were well characterized by X-ray diffraction (XRD), field emission scanning electron microscopy (FESEM), transmission electron microscopy (TEM), and energy dispersive X-ray spectroscopy (EDS). The photocatalytic activities were evaluated in the degradation of methylene blue (MB) aqueous solution. The results showed that Ag_2O nanoparticles sized 3-10 nm were highly anchored on the surface and inner tubes of the N-HCNTs support, and significantly enhanced the visible-light photocatalytic activity compared to bare Ag_2O. It was attributed to the combined effects, including highly dispersed smaller Ag_2O particles and higher charge separation efficiency. The possible mechanism for the photocatalytic activity of Ag_2O/N-HCNTs was also tentatively proposed. In particular, the rate of degradation of the as-prepared Ag_2O/N-HCNTs was 3.9 times faster than that of using bare Ag_2O nanoparticles under visible light irradiation. Furthermore, the Ag_2O/N-HCNTs could be easily recycled in visible photocatalytic activity. In addition, the Ag_2O/N-HCNTs could also degrade MB dye in different water sources like

* Corresponding author. Tel.: +86 25 52090617; fax: +86 25 52090617.
E-mail address: ymzhou@seu.edu.cn (Yuming Zhou).
‡ J.J. Xue and S.S. Ma contributed equally to this work.

Changjiang river water and tap water with high efficiency as well as in deionized water and that will greatly promote their application in the area of environmental remediation.

Introduction

In decades, the environmental problem caused by organic pollutants has increased with the rapid development of industry and become a severe threat to human beings.[1-4] With the steady and fast growing field of nanoscience and nanotechnology, semiconductor photocatalysts based on harnessing and converting solar energy into chemical energy are attracting increasing attention because of their potential applications in solving environmental pollution.[5-10] Among the semiconductors, titanium dioxide (TiO_2), owing to its low cost, ease in preparation, environmental abundance, high photocatalytic activity, good chemical stability, and nontoxicity, is considered to be one of the most important semiconductors being harnessed in photoinduced applications such as photodetection and photocatalysis.[11, 12] However, due to the large band gap (3.2 eV) of TiO_2, it only can be excited under UV light irradiation. Meanwhile, visible-light makes up about 45% of solar energy and UV light only around 4%, the development of visible-light-responsive photocatalysts for environmental remediation has become an active area of research in photocatalysis.[13-16] Recently, silver-containing compounds have been demonstrated to be efficient photocatalytic materials under visible-light irradiation.[17-21] Among the silver-containing compounds, Ag_2O is a well-known visible light photocatalyst which shows excellent photocatalytic performance and good stability.[22-24] However, the consumption of a large amount of the noble metal of silver strongly limits their practical environmental applications despite the fact that Ag_2O photocatalyst exhibited highly efficient in visible-light photocatalytic performance. On the

other hand, the particle size of Ag_2O photocatalyst remains relatively large, which hinder their performance in visible photocatalytic processes.[23, 25] Therefore, it should develop a simple and effective technology to reduce the dosage of silver and to synthesize nanosized Ag_2O photocatalyst with high efficient photocatalytic activity for large-scale practical applications.

Carbonaceous materials, such as carbon quantum dots, activated carbon, carbon black, and carbon nanotubes, have been demonstrated to be good supports for semiconductor photocatalysts due to their range of light absorption, cheapness, safety, and corrosion resistance.[26-29] Among them, one-dimensional carbon nanotubes (CNTs) have been widely used as ideal electron pathways due to their special one-dimensional (1D) character and good conductivity. And some results have demonstrated that CNTs could efficiently capture and transport of photogenerated electrons through highly conductive long CNTs.[30-32] In particular, helical carbon nanotubes (HCNTs), have aroused special attention since they were observed by Amelinckx et al. in 1994 based on their outstanding physical and chemical properties and potential applications.[33] It is found that HCNTs exhibit unique electrical and mechanical properties that could be utilized in nanoengineering.[34-37] The specific helical geometry (such as diameter and coil pitch, etc.) is determined by the periodic incorporation of pentagon and heptagon pairs in hexagonal carbon network.[34] Interestingly, depending on the helical geometry, a HCNT can behave as a semiconductor, a semimetal, a metal, or even a superconductor, which is impossible in the case of straight CNTs.[38] Moreover, because doping nitrogen into carbon materials could be a promising way to improve their electronic, mechanical, and optical properties, many efforts have been devoted to study N-doped HCNTs (N-HCNTs).[36, 37, 39-41] In addition, the introduction of nitrogen into carbon materials could

create more active sites for anchoring functional metal or metallic oxide nanoparticles.[42] Judging from the excellent visible photocatalyst of Ag_2O and the efficient electron transfer property of N-HCNTs, combination of Ag_2O and N-HCNTs seems to be ideal for hindering the recombination of photogenerated electrons (e^-) and holes (h^+) and improving the photocatalytic efficiency. Besides, to our best of knowledge, there have been no reports on the synthesis and photocatalytic activity of the Ag_2O/N-HCNTs under visible light.

Herein, for the first time, the Ag_2O/N-HCNTs sample was prepared via a simple adsorption and coprecipitation method using N-HCNTs as the support material at room temperature. The results indicated that Ag_2O was anchored on the surface and inner tubes of N-HCNTs with size about 3-10 nm, causing the composite to display stronger visible absorption and to exhibit enhanced photocatalytic activities for the degradation of methylene blue (MB) under visible light compared with separate N-HCNTs and Ag_2O. Moreover, Ag_2O/N-HCNTs sample could be easily recycled in visible photocatalytic activity and remove dyes in living water samples such as tap water and Changjiang River water with high efficiency as well as in deionized water.

Experimental section

Materials: Pyrrole, ammonium persulfate (APS), silver nitrate ($AgNO_3$), ethanol (EtOH), methanol (MeOH), sodium hydroxide (NaOH) and methylene blue (MB, $C_{16}H_{18}ClN_3S$) were purchased from Aladdin Chemical Regent Co., Ltd. (Shanghai, China). All the reagents in this experiment are analytically pure and used without further purification.

Synthesis of N-HCNTs: The preparation of N-HCNTs is similar to the method described by Liu *et al*.[43] N-HCNTs were prepared with the template of C_{14}-L-Glu, which was

synthesized from myristoyl chloride and L-glutamic acid in a mixture of water and acetone as descried previously. [44, 45] Typically, 0.3 mmol of C_{14}-L-Glu was dissolved in 65 mL of MeOH at room temperature, then 12 mmol of pyrrole and 300 mL of deionized water were added. The aforementioned mixture was stirred for 30 min. Subsequently, 6 mL of APS solution (2 M) was added into the mixture and stirred for another 60 min at room temperature, yielding a dark suspension. Finally, a dark precipitation was collected and washed thoroughly with deionized water and ethanol for several times and finally dried under vacuum. Then the resulting dark product was calcined at 550 ^{o}C under a flow of N_2 for 6 h. After slowly cooling to room temperature, N-HCNTs sample was obtained.

Formation of Ag_2O/N-HCNTs: Typically, 0.03 g of N-HCNTs were dispersed in 300 mL of deionized water by sonication for 60 min to form a uniformly suspension. Subsequently, 0.15 g of $AgNO_3$ was added into the above suspension. After stirring for another 120 min, 15 mL aqueous solution of NaOH (0.5 M) was added to the aforementioned mixture and then stirred for another 30 min. The obtained precipitate was separated by centrifugation and washed thoroughly with deionized water and ethanol for several times to remove any impurities. Finally, the product was dried in vacuum at 45 °C for 12 h. For comparison, bare Ag_2O was also synthesized in the same way but in the absence of N-HCNTs.

Characterization

The field emission scanning electron microscopy (FESEM; FEI Inspect F50), transmission electron microscopy (TEM; JEM-1230) and high resolution TEM (HRTEM) were used to characterize the morphologies of the products. Energy dispersive X-ray

spectroscopy (EDS) being attached to field emission scanning electron microscopy (FESEM) was used to analyze the composition of samples. X-ray diffraction (XRD) measurement was carried out using a SmartLab XRD spectrometer (Rigaku) with Cu Kα radiation in the range of 10-70° (2θ). The nitrogen adsorption and desorption isotherms were measured at 77 K on an ASAP 2020 (Micromertics USA). UV-vis diffuse reflectance spectra (DRS) of the samples were recorded on a UV-vis spectrophotometer (UV-3600, Shimadzu) with an integrating sphere attachment.

Evaluation of Photocatalytic Performance

The photodegradation of MB was chosen as a model reaction to evaluate the photocatalytic activities of the Ag_2O/N-HCNTs. A 500 W xenon lamp (Philips) equipped with a UV cut-off filter with $\lambda > 400$ nm was used as the light source. The experiments were carried out at room temperature as follows: the photocatalyst (50 mg) was added to a 100 mL of MB aqueous solution (10 mg/L) in a Pyrex reactor. Before irradiation, the mixed suspension was stirred for 30 min in the dark to reach an adsorption-desorption equilibrium between the photocatalyst and MB dye. Subsequently, the above mixture was irradiated in a photochemical chamber under continuously stirring with reflux water to keep its temperature constant. At intervals of 30 min, 3 mL of the suspension was collected and centrifuged to remove the remnant photocatalyst. The concentration of MB in the supernatant was then performed by measuring its intensity of the absorption peak with a UV-vis spectrophotometer (UV-3600; Shimadzu). For comparison, the photocatalytic activities of bare Ag_2O and N-HCNTs were also determined under identical conditions.

Results and discussion

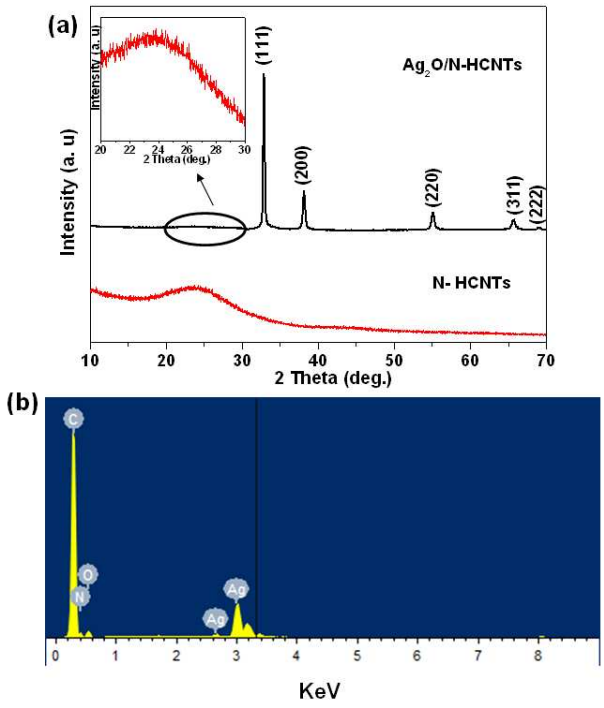

Fig. 1 XRD patterns of the as-prepared (a) N-HCNTs and Ag_2O/N-HCNTs, (b) EDS spectrum of the Ag_2O/N-HCNTs.

Structure and Morphology

X-ray diffraction (XRD) analysis was employed to investigate the phase structure of the as-synthesized samples. As shown in Fig. 1(a), the N-HCNTs sample shows a broad peak and the diffraction peak at 24.6° corresponds to *d* spacing of 0.36 nm.[46] In the diffraction patterns of the as-prepared Ag_2O/N-HCNTs, the major diffraction peaks at 2θ = 32.8°, 38.1°, 54.9°, 65.4° and 68.7° are in accordance with the standard data of well-crystallized cubic Ag_2O (JCPDS 41-1104). Meanwhile, the weak and broad peak in the range of 20°~30° (inset of Fig. 1(a)) originates from the N-HCNTs sample. No characteristic peaks for other impurities were observed, which indicated that the product had high purity. And the EDS analysis (Fig. 1(b)) further confirms that the product was only composed of C, N, O and Ag.

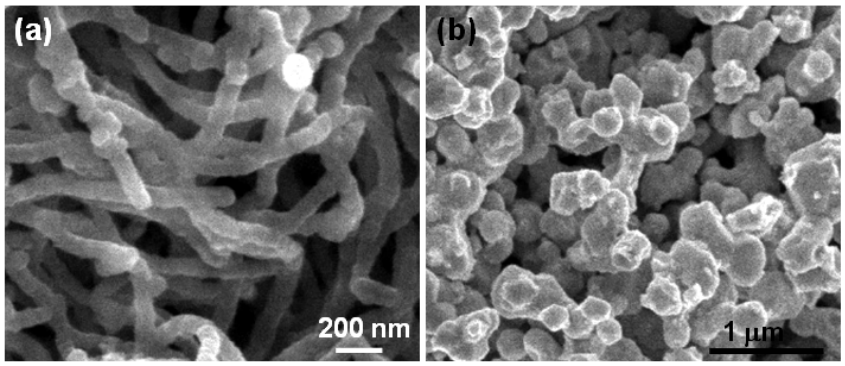

Fig. 2 FESEM images of bare (a) N-HCNTs and (b) Ag_2O nanoparticles.

The sizes, morphologies, and microstructures of the as-prepared N-HCNTs, bare Ag_2O and Ag_2O/N-HCNTs were elucidated by field emission scanning electron microscopy (FESEM), transmission electron microscopy (TEM) and high resolution TEM (HRTEM). Fig.2 (a, b) shows representative FESEM images of the synthesized N-HCNTs and bare Ag_2O. And Fig. 3 shows the typical TEM and HRTEM images of bare N-HCNTs, individual N-HCNT and Ag_2O/N-HCNTs, respectively. As seen from Fig. 2(a) and Fig. 3(a), the N-HCNTs sample is composed of exclusively left-handed helical fibers with uniform morphology. The outer diameters of N-HCNTs are in the same range of 70-100 nm and in length of several micrometers. The pitches of outer surface along the rod axis are estimated to be all about 80 nm, as indicated by black arrows in Fig. 3(b). In Fig. 2(b), it can be clearly seen that the Ag_2O nanoparticles possess an irregular spherical morphology with an average diameter of approximately 100 nm. In contrast, from Fig. 3(c), the Ag_2O nanoparticles are clearly and uniformly anchored on the surface and inner tubes of N-HCNTs to form Ag_2O/N-HCNTs, which is propitious to electron transmission between two phases. By measuring the lattice fringes in HRTEM image (Fig. 3(d)), the resolved interplanar distance of 0.235 nm which enlarged inset of Fig. 3(d) agreed well with the lattice spacing of the plane of

Ag_2O. This is indicative of the formation of Ag_2O/N-HCNTs. Compared with the bare Ag_2O nanoparticles prepared in the absence of N-HCNTs, the Ag_2O particles in the Ag_2O/N-HCNTs hybrid are smaller with diameters in the range of 3-10 nm (Fig. 3(d)). The smaller size of the Ag_2O nanoparticles may be attributed to the existence of N-HCNTs in the Ag_2O/N-HCNTs systems, which probably provide a platform to prevent the agglomeration of Ag_2O particles.

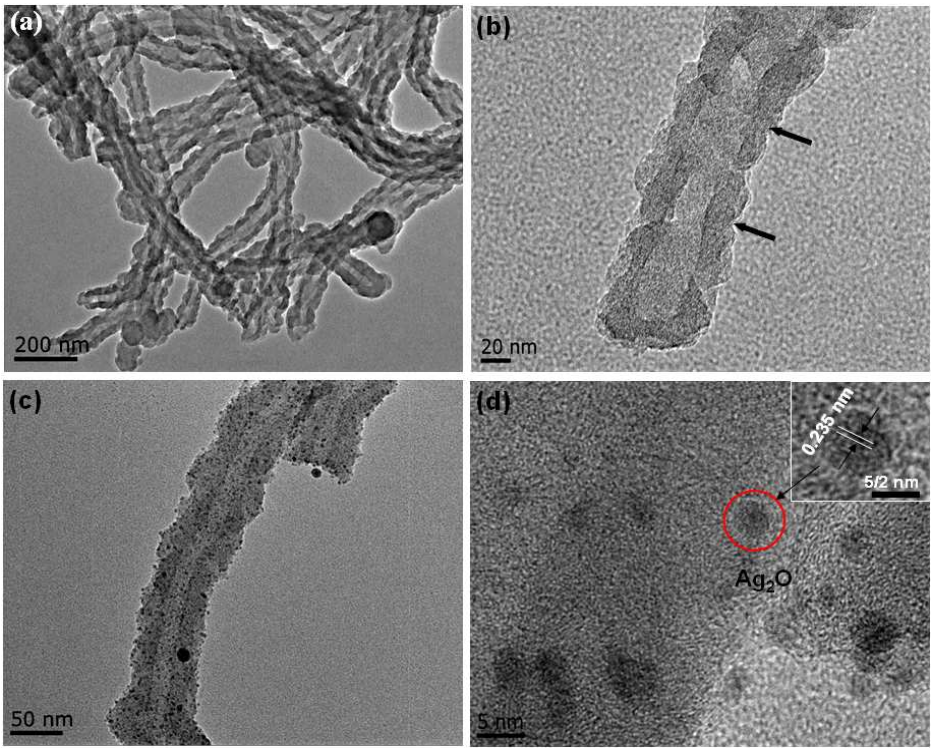

Fig. 3 Typical TEM images of (a) bare N-HCNTs, (b) an individual N-HCNT and (c) Ag_2O/N-HCNTs; (d) HRTEM image of Ag_2O/N-HCNTs. Inserts in (d) is the enlarged image.

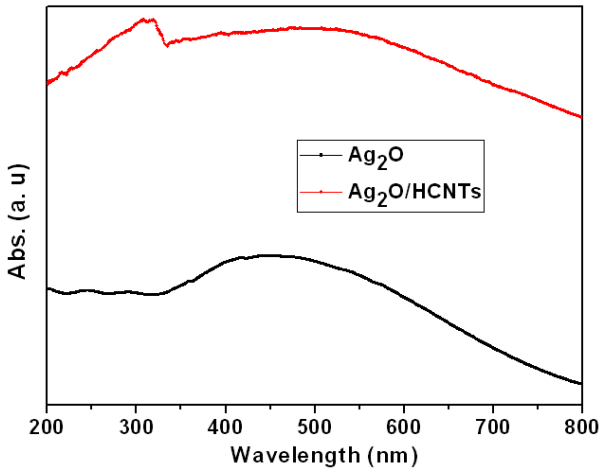

Fig. 4 UV/Vis diffuse reflectance spectra of bare Ag_2O and Ag_2O/N-HCNTs.

It is well known that optical absorption plays an important role in determining the photocatalytic performance of a catalyst, especially in the visible-light photodegradation of contaminants.[47, 48] The optical properties of bare Ag_2O and Ag_2O/N-HCNTs were probed by UV/Vis diffuse reflectance spectroscopy (Fig. 4). The UV/Vis spectrum of the as-prepared Ag_2O clearly exhibits broad and strong absorption intensity in the whole UV and visible-light region of 200-800 nm, which is in agreement with previous reports.[22] The Ag_2O/N-HCNTs nanocomposites exhibit more intense in the range of 200-800 nm than that of bare Ag_2O, which suggests that the Ag_2O/N-HCNTs photocatalyst may absorb visible light more efficiently. An analogous phenomenon has also been reported by other researchers.[49, 50]

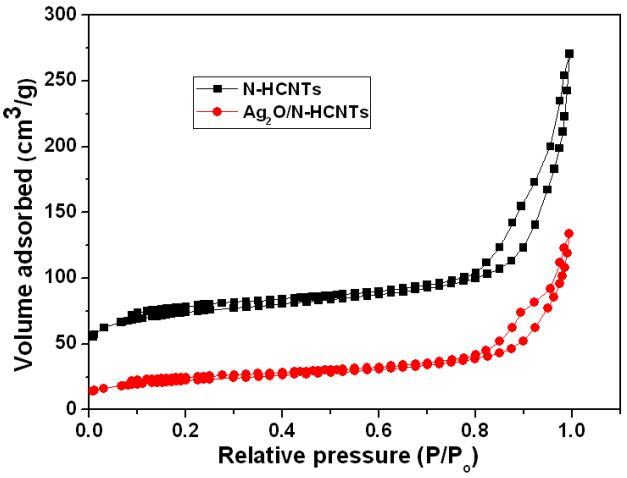

Fig. 5 N_2 adsorption-desorption isotherms of N-HCNTs and Ag_2O/N-HCNTs.

The nitrogen adsorption-desorption isotherms of N-HCNTs and Ag_2O/N-HCNTs are shown in Fig. 5. It can be seen that both of the N-HCNTs and Ag_2O/N-HCNTs samples show a type IV adsorption isotherm and H3 hysteresis loop, indicating the presence of mesoporous (2-50 nm). [51, 52] The BET surface area and the single-point total pore volume for N-NCNTs came out to be 272.6 $m^2 \bullet g^{-1}$ and 0.42 $cm^3 \bullet g^{-1}$, respectively. The average BJH pore diameter calculated from the desorption branch of the isotherms was determined to be 11 nm. However, the values for the BET surface area, total pore volume, and pore diameter of the Ag_2O/N-HCNTs sample was calculated at 78 $m^2 \bullet g^{-1}$, 0.21 $cm^3 \bullet g^{-1}$, and 14.1 nm, respectively. Compared with N-HCNTs, the Ag_2O/N-HCNTs sample show a monotonic decrease in BET surface areas and pore volumes and increase in average pore size. This is probably caused by the heavy coating of the N-HCNTs by small crystallite size of Ag_2O nanoparticles.[53]

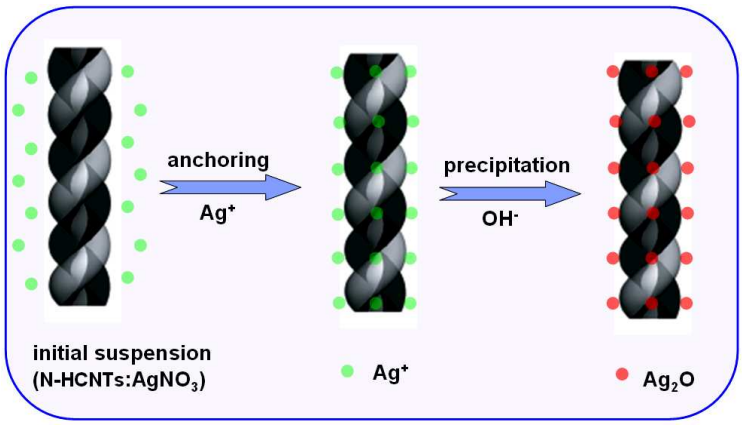

Scheme 1 Schematic illustration of the fabrication route of Ag_2O/N-HCNTs.

Formation mechanism of Ag_2O/N-HCNTs

Based on the above results, we speculated a possible formation mechanism for the preparation of Ag_2O/N-HCNTs, as illustrated in Scheme 1. In the previous reports, the incorporation of nitrogen atoms into CCNTs could create more active sites for anchoring functional metal nanoparticles, such as Pt and Ag, thus resulting in the use of CCNTs as novel supports of catalysts for direct methanol fuel cells (DMFC), bactericides, and sensors.[46, 54] Herein, the fabrication of Ag_2O/N-HCNTs is based on the anchoring of positively charged Ag^+ ions on the surface and inner tubes of N-HCNTs, and followed by subsequent in situ growth of Ag_2O.

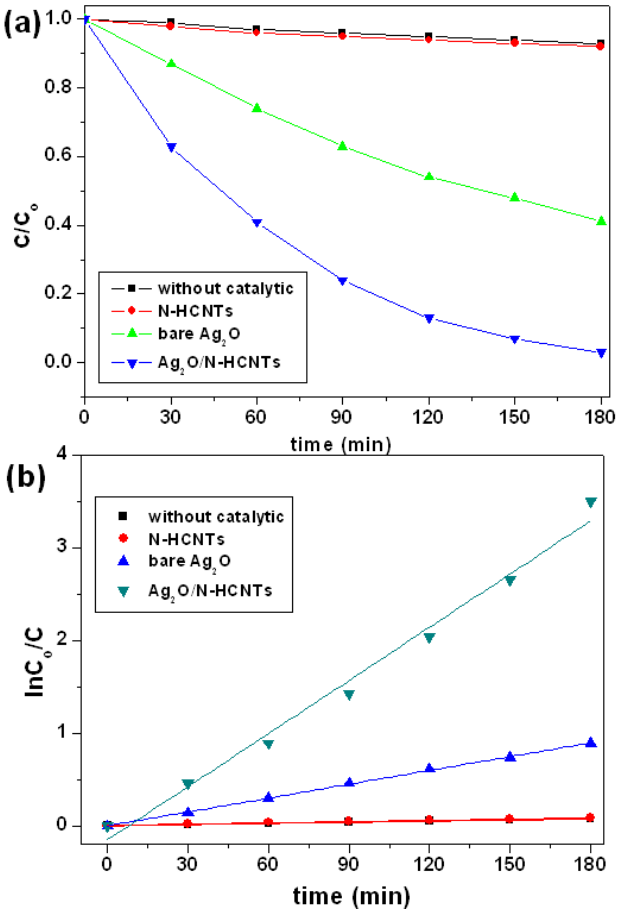

Fig. 6 Photocatalytic activity (a) and kinetics (b) of the as-prepared Ag_2O/N-HCNTs, N-HCNTs, and bare Ag_2O for degradation of MB under visible light irradiation.

Photocatalytic Activity

The photcatalytic performances in UV and visible light regions were investigated via the degradation of MB, which is a typical cationic organic pollutant usually discharged by the textile industry after used. According to the Beer-Lambert law, the concentration of MB is linearly proportional to the intensity of the absorption peak at 664 nm, and thus the decomposition efficiency of MB can be calculated using the following expression:

$$\text{MB decomposition (\%)} = 100 \times (C_o - C) / C_o \quad (1)$$

Where, C_o and C are the equilibrium concentrations of MB before and after UV

irradiation, respectively. Fig. 6(a) shows the photocatalytic decomposition of MB monitored according to the concentration change versus time for the various samples. As can be seen, the concentrations of the MB solution are almost unchanged in the absence of any catalyst or with bare N-HCNTs. However, it is noticeable that the Ag_2O/N-HCNTs composite exhibit significantly enhanced activity compared with bare Ag_2O and N-HCNTs. After 180 min of visible light irradiation, the photodegradation efficiency of Ag_2O/N-HCNTs nearly reach 97 %, while the bare Ag_2O and N-HCNTs can only approach 59 % and 8 % for the same irradiation time, respectively. Furthermore, to quantitatively understand the reaction kinetics of MB degradation over different samples in our experiments, we re-plotted the data in Fig. 5(b) according to the pseudo-first-order kinetic model as expressed by equation (2), which is generally used for photocatalytic degradation process take place at the interface between the catalysts and the organic pollutants with low concentration.

$$\ln (C_o/C) = kt \qquad (2)$$

Where, t is reaction time, k is the rate constant, C_o and C are the concentrations of MB solution at time 0 and t, respectively.[55] From Fig. 6(b), the rate constants of Ag_2O/N-HCNTs, bare Ag_2O and N-HCNTs are 0.0195 min^{-1}, 0.005 min^{-1} and 0.0005 min^{-1}, respectively. The Ag_2O/N-HCNTs exhibit the highest rate constant, which is approximately 3.9 times larger than that of pure Ag_2O. The enhanced photocatalytic activities were attributed to combined effects, including the highly dispersed smaller Ag_2O particles and the higher separation efficiency of photoinduced electron-hole pairs based on the exist of N-HCNTs.

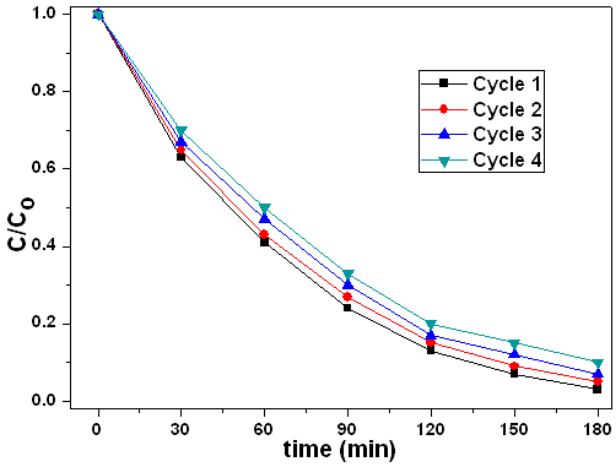

Fig. 7 Four photocatalytic degradation cycles of MB using Ag_2O/N-HCNTs under visible light irradiation.

To investigate the stability of photocatalytic performance in visible light region, the as-prepared Ag_2O/N-HCNTs were used to degrade MB dye in four repeated cycles, and the results are shown in Fig. 7. It is noteworthy that the photocatalytic performance of the as-prepared Ag_2O/N-HCNTs exhibit effective photostability under visible light irradiation, where the photocatalytic efficiency reduces only by 8 % after four cycles, indicate that the good stability of the Ag_2O/N-HCNTs photocatalyst.

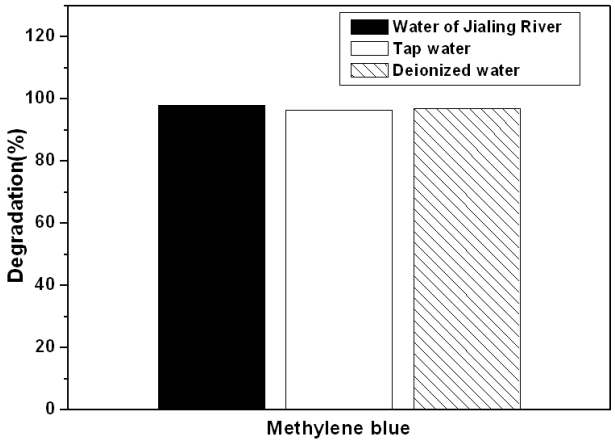

Fig. 8 Photocatalytic activity of the as-prepared Ag_2O/N-HCNTs for degradation of MB in different water sources under visible light irradiation.

For further practical applications, Fig. 8 shows the photocatalytic activity of the

as-prepared Ag_2O/N-HCNTs for degradation of MB in different water sources under visible light irradiation. Firstly, MB was added into tap water and Changjiang River water to form different MB solutions with the same concentration in deionized water. Then, the as-prepared Ag_2O/N-HCNTs were added into different MB solutions, followed by the same photocatalytic experiment steps mentioned above. As can be seen from Fig 8, the as-prepared Ag_2O/N-HCNTs almost exhibit the same photocatalytic activity in different water sources under visible light irradiation, suggesting that this sample was suitable for removal of dyes from different water sources. It is also indicated that the as-prepared Ag_2O/N-HCNTs have great potential applications for pollution control in our environment.

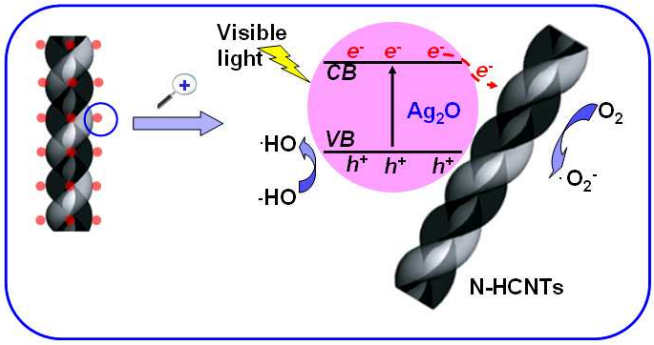

Fig. 9 Proposed mechanism for the photocatalytic degradation of MB over Ag_2O/N-HCNTs under visible-light irradiation.

Mechanisms in Enhancing Photocatalytic Activity

Based on the results above, a possible photocatalytic mechanism of the as-prepared Ag_2O/N-HCNTs under visible light irradiation was proposed and illustrated in Fig. 9. The mechanism was that the N-HCNTs supported catalysts were believed to exhibit cooperative or synergetic effects between N-HCNTs and semiconductive metal oxides. The work function of CNTs has been computed to be ranging from 4.3 to 5.1 eV,[56] Ag_2O semiconductor has the conduction band *ca.* 0.19 eV and a band gap of about 1.2 eV.[57] The conducting band of Ag_2O

is smaller than work functions of CNTs, such that the photogenerated electrons transfer from Ag_2O to CNTs is energetically favorable.[58] Here, when the as-prepared Ag_2O/N-HCNTs were irradiated with visible light, Ag_2O could be excited due to its narrow band gap (1.2 eV) and the photogenerated electrons (e^-) were produced in the conduction band (CB) while the photogenerated holes (h^+) remained in the valence band (VB).[59] Subsequently, photogenerated electrons (e^-) in Ag_2O conduction band (CB) might move freely toward the surface of the N-HCNTs and excess of valence band holes were left in the Ag_2O to migrate to the surface and react with H_2O or OH^- to produce active species such as OH•,[26] suggesting that the photogenerated electrons and holes were efficiently separated and the lifetime of the excited electrons and holes could be prolonged in the transfer process. Thus, the lifetime of the excited electrons and holes can be prolonged in the transfer process, inducing higher quantum efficiency, and thus the photocatalytic activity of the as-prepared Ag_2O/N-HCNTs is enhanced greatly. The mechanism for the photocatalytic degradation of MB in our experiment was proposed as follows:

$$Ag_2O/\text{N-HCNTs (s)} + h\nu \rightarrow h^+ (Ag_2O) + e^- (\text{N-HCNTs})$$

$$e^- + O_2 \rightarrow O_2\bullet^-$$

$$h^+ + OH^- \rightarrow OH\bullet$$

$$O_2\bullet^- + H_2O \rightarrow HO_2\bullet + OH\cdot$$

$$HO_2\bullet + H_2O \rightarrow H_2O_2 + OH\cdot$$

$$H_2O_2 \rightarrow 2OH\bullet$$

$$OH\bullet + \text{MB (dye)} \rightarrow CO_2 + H_2O$$

$$h^+ + \text{MB (dye)} \rightarrow CO_2 + H_2O$$

Under visible-light irradiation, photogenerated electrons (e^-) in Ag_2O moved freely to the surface of the N-HCNTs. Meanwhile, the photogenerated holes (h^+) were left in the valence band of Ag_2O. Subsequent to various steps, the photogenerated holes (h^+) were ultimately trapped by surface hydroxyl groups (or H_2O) on the surface of catalyst to yield OH• radicals. Simultaneously, the dissolved oxygen molecules react with the surface of the N-HCNTs photogenerated electrons (e^-) to yield super oxide radical anions (O_2•-), which on protonation generate the hydroperoxy (HO_2•) radicals, producing hydroxyl radical OH•, which was a strong oxidizing agent to decompose organic dye.[60]

Conclusions

In summary, Novel visible-light-responsive Ag_2O/N-HCNTs have been successfully synthesized by a simple coprecipitation route. The Ag_2O nanoparticles were evenly and densely distributed over the surface and inner tubes of N-HCNTs. The incorporation of Ag_2O in N-HCNTs can promote the formation of Ag_2O nanoparticles with a smaller size and significantly enhance the photocatalytic activity of the composite catalysts in the degradation of the contaminant MB under visible-light irradiation. The enhanced photocatalytic activity of the Ag_2O/N-HCNTs can be attributed to the synergic effect of the effective separation of the photogenerated carriers and the smaller particle size of Ag_2O when coupled with the N-HCNTs. In addition, the Ag_2O/N-HCNTs could be easily recycled in visible photocatalytic activity and degrade MB dye in different water sources such as Changjiang river water and tap water with high efficiency as well as in deionized water. The high and stable catalytic activity makes the Ag_2O/N-HCNTs promising photocatalysts for the resolution of energy and environmental issues.

Acknowledgements

The authors are grateful to National Natural Science Foundation of China (Grant No. 21106017 and 51077013), Fund Project for Transformation of Scientific and Technological Achievements of Jiangsu Province of China (Grant No. BA2011086), Specialized Research Fund for the Doctoral Program of Higher Education of China (Grant No.20100092120047) and Key Program for the Scientific Research Guiding Found of Basic Scientific Research Operation Expenditure of Southeast University (Grant No.3207042102).

References

1. C. C. Chen, W. H. Ma and J. C. Zhao, *Chem. Soc. Rev.*, 2010, **39**, 4206-4219.
2. D. Q. Zhang, M. C. Wen, B. Jiang, G. S. Li and J. C. Yu, *J. Hazard. Mater.*, 2012, **211**, 104-111.
3. M. A. Shannon, P. W. Bohn, M. Elimelech, J. G. Georgiadis, B. J. Marinas and A. M. Mayes, *Nature*, 2008, **452**, 301-310.
4. C. J. Vorosmarty, P. B. McIntyre, M. O. Gessner, D. Dudgeon, A. Prusevich, P. Green, S. Glidden, S. E. Bunn, C. A. Sullivan, C. R. Liermann and P. M. Davies, *Nature*, 2010, **467**, 555-561.
5. A. Kudo and Y. Miseki, *Chem. Soc. Rev.*, 2009, **38**, 253-278.
6. S. A. K. Leghari, S. Sajjad, F. Chen and J. L. Zhang, *Chem. Eng. J.*, 2011, **166**, 906-915.
7. X. Xu, X. P. Shen, H. Zhou, D. Z. Qiu, G. X. Zhu and K. M. Chen, *Appl. Catal. a-Gen.*, 2013, **455**, 183-192.
8. N. Watanabe, T. Kaneko, Y. Uchimaru, S. Yanagida, A. Yasumori and Y. Sugahara, *Crystengcomm*, 2013, **15**, 10533-10540.

9. H. B. Lu, S. M. Wang, L. Zhao, J. C. Li, B. H. Dong and Z. X. Xu, *J. Mater. Chem.*, 2011, **21**, 4228-4234.

10. S. S. Ma, R. Li, C. P. Lv, W. Xu and X. L. Gou, *J. Hazard. Mater.*, 2011, **192**, 730-740.

11. X. Zhang, V. Thavasi, S. G. Mhaisalkar and S. Ramakrishna, *Nanoscale*, 2012, **4**, 1707-1716.

12. M. M. Khan, S. A. Ansari, D. Pradhan, M. O. Ansari, D. H. Han, J. Lee and M. H. Cho, *J. Mater. Chem. A*, 2014, **2**, 637-644.

13. J. G. Yu, J. Jin, B. Cheng and M. Jaroniec, *J. Mater. Chem. A*, 2014, **2**, 3407-3416.

14. X. X. Wei, C. M. Chen, S. Q. Guo, F. Guo, X. M. Li, X. X. Wang, H. T. Cui, L. F. Zhao and W. Li, *J. Mater. Chem. A*, 2014, **2**, 4667-4675.

15. X. J. Feng, T. J. LaTempa, J. I. Basham, G. K. Mor, O. K. Varghese and C. A. Grimes, *Nano Lett.*, 2010, **10**, 948-952.

16. Z. Y. Liu, D. D. L. Sun, P. Guo and J. O. Leckie, *Nano Lett.*, 2007, **7**, 1081-1085.

17. H. Kato, H. Kobayashi and A. Kudo, *J. Phys. Chem. B*, 2002, **106**, 12441-12447.

18. R. Konta, H. Kato, H. Kobayashi and A. Kudo, *Phys. Chem. Chem. Phys.*, 2003, **5**, 3061-3065.

19. T. Kako, N. Kikugawa and J. Ye, *Catal. Today*, 2008, **131**, 197-202.

20. P. Wang, B. B. Huang, X. Y. Qin, X. Y. Zhang, Y. Dai, J. Y. Wei and M. H. Whangbo, *Angew. Chem. Int. Edit.*, 2008, **47**, 7931-7933.

21. D. W. Wang, Y. Li, G. L. Puma, C. Wang, P. F. Wang, W. L. Zhang and Q. Wang, *Chem. Commun.*, 2013, **49**, 10367-10369.

22. X. F. Wang, S. F. Li, H. G. Yu, J. G. Yu and S. W. Liu, *Chem. Eur. J.*, 2011, **17**, 7777-7780.

23. Z. Y. Ji, X. P. Shen, J. L. Yang, Y. L. Xu, G. X. Zhu and K. M. Chen, *Eur. J. Inorg. Chem.*,

2013, **2013**, 6119-6125.

24. G. Wang, X. C. Ma, B. B. Huang, H. F. Cheng, Z. Y. Wang, J. Zhan, X. Y. Qin, X. Y. Zhang and Y. Dai, *J. Mater. Chem.*, 2012, **22**, 21189-21194.

25. L. Shi, L. Liang, J. Ma, F. X. Wang and J. M. Sun, *Catal. Sci. Technol.*, 2014, **4**, 758-765.

26. K. Woan, G. Pyrgiotakis and W. Sigmund, *Adv. Mater.*, 2009, **21**, 2233-2239.

27. Q. H. Liang, Y. Shi, W. J. Ma, Z. Li and X. M. Yang, *Phys. Chem. Chem. Phys.*, 2012, **14**, 15657-15665.

28. B. Y. Yu and S. Y. Kwak, *J. Mater. Chem.*, 2012, **22**, 8345-8353.

29. J. B. Mu, C. L. Shao, Z. C. Guo, Z. Y. Zhang, M. Y. Zhang, P. Zhang, B. Chen and Y. C. Liu, *Acs Appl. Mater. Inter.*, 2011, **3**, 590-596.

30. H. E. Unalan, D. Wei, K. Suzuki, S. Dalal, P. Hiralal, H. Matsumoto, S. Imaizumi, M. Minagawa, A. Tanioka, A. J. Flewitt, W. I. Milne and G. A. J. Amaratunga, *Appl. Phys. Lett.*, 2008, **93**, 133116-1-133116-3.

31. S. Da Dalt, A. K. Alves and C. P. Bergmann, *Mater. Res. Bull.*, 2013, **48**, 1845-1850.

32. S. H. Wang and S. Q. Zhou, *J. Hazard. Mater.*, 2011, **185**, 77-85.

33. S. Amelinckx, X. B. Zhang, D. Bernaerts, X. F. Zhang, V. Ivanov and J. B. Nagy, *Science*, 1994, **265**, 635-639.

34. K. Akagi, R. Tamura, M. Tsukada, S. Itoh and S. Ihara, *Phys. Rev. Lett.*, 1995, **74**, 2307-2310.

35. A. Volodin, D. Buntinx, M. Ahlskog, A. Fonseca, J. B. Nagy and C. Van Haesendonck, *Nano Lett.*, 2004, **4**, 1775-1779.

36. J. F. Wen, Y. Zhang, N. J. Tang, X. G. Wan, Z. H. Xiong, W. Zhong, Z. L. Wang, X. L. Wu and Y. W. Du, *J. Phys. Chem. C*, 2011, **115**, 12329-12334.

37. Y. Liu, N. J. Tang, W. Kuo, C. W. Jiang, J. F. Wen and Y. W. Du, *J. Phys. Chem. C*, 2012, **116**, 14584-14590.

38. D. M. Chen, K. W. Wang, D. G. Xiang, R. L. Zong, W. Q. Yao and Y. F. Zhu, *Appl. Catal. B-Environ.*, 2014, **147**, 554-561.

39. Y. Ganesan, C. Peng, Y. Lu, L. Ci, A. Srivastava, P. M. Ajayan and J. Lou, *Acs Nano*, 2010, **4**, 7637-7643.

40. P. Ayala, R. Arenal, M. Rummeli, A. Rubio and T. Pichler, *Carbon*, 2010, **48**, 575-586.

41. K. Xiao, Y. Fu, Y. Q. Liu, G. Yu, J. Zhai, L. Jiang, W. P. Hu, Z. G. Shuai, Y. Luo and D. B. Zhu, *Adv. Funct. Mater.*, 2007, **17**, 2842-2846.

42. L. L. Wang, L. Shen, L. P. Zhu, H. Y. Jin, N. C. Bing and L. J. Wang, *J Nanomater.*, 2012, (doi: 10.1155/2012/794625).

43. S. H. Liu, Y. Y. Duan, X. J. Feng, J. Yang and S. A. Che, *Angew. Chem. Int. Edit.*, 2013, **52**, 6858-6862.

44. Y. J. Zhang, Y. L. Song, Y. Y. Zhao, T. J. Li, L. Jiang and D. B. Zhu, *Langmuir*, 2001, **17**, 1317-1320.

45. M. Takehara, K. Takizawa, Yoshimur.I and R. Yoshida, *J. Am. Oil Chem. Soc.*, 1972, **49**, 157-161.

46. Y. W. Ma, S. J. Jiang, G. Q. Jian, H. S. Tao, L. S. Yu, X. B. Wang, X. Z. Wang, J. M. Zhu, Z. Hu and Y. Chen, *Energ. Environ. Sci.*, 2009, **2**, 224-229.

47. N. Zhang, Y. H. Zhang and Y. J. Xu, *Nanoscale*, 2012, **4**, 5792-5813.

48. Y. H. Zhang, Z. R. Tang, X. Z. Fu and Y. J. Xu, *Acs Nano*, 2010, **4**, 7303-7314.

49. G. Z. Liao, S. Chen, X. Quan, H. T. Yu and H. M. Zhao, *J. Mater. Chem.*, 2012, **22**,

2721-2726.

50. J. C. Liu, H. W. Bai, Y. J. Wang, Z. Y. Liu, X. W. Zhang and D. D. Sun, *Adv. Funct. Mater.*, 2010, **20**, 4175-4181.

51. K. S. W. Sing, D. H. Everett, R. A. W. Haul, L. Moscou, R. A. Pierotti, J. Rouquerol and T. Siemieniewska, *Pure Appl. Chem.*, 1985, **57**, 603-619.

52. A. Hebrard, D. Oulahna, L. Galet, B. Cuq, J. Abecassis and J. Fages, *Powder Technol.*, 2003, **130**, 211-218.

53. J. G. Yu and J. Zhang, *Dalton T.*, 2010, **39**, 5860-5867.

54. A. Zamudio, A. L. Elias, J. A. Rodriguez-Manzo, F. Lopez-Urias, G. Rodriguez-Gattorno, F. Lupo, M. Ruhle, D. J. Smith, H. Terrones, D. Diaz and M. Terrones, *Small*, 2006, **2**, 346-350.

55. M. S. Lee, S. S. Park, G. D. Lee, C. S. Ju and S. S. Hong, *Catal. Today*, 2005, **101**, 283-290.

56. H. Ago, T. Kugler, F. Cacialli, W. R. Salaneck, M. S. P. Shaffer, A. H. Windle and R. H. Friend, *J. Phys. Chem. B*, 1999, **103**, 8116-8121.

57. Y. Xu and M. A. A. Schoonen, *Am. Mineral.*, 2000, **85**, 543-556.

58. C. X. Guo, H. B. Yang, Z. M. Sheng, Z. S. Lu, Q. L. Song and C. M. Li, *Angew. Chem. Int. Edit.*, 2010, **49**, 3014-3017.

59. S. S. Ma, J. J. Xue, Y. M. Zhou and Z. W. Zhang, *J. Mater. Chem. A*, 2014, **2**, 7272-7280.

60. T. Aarthi and G. Madras, *Ind. Eng. Chem. Res.*, 2007, **46**, 7-14.